A Study of Stablized Nanoscale Austenite in a Low-Alloy Medium-Carbon Steel

R. Jafari[1], Sh. Mirdamadi[1], Sh. Kheirandish[1] and H. U. Guim[2]

* *kheirandish@iust.ac.ir*

Received: January 2018 Accepted: April 2018

[1] School of Metallurgy and Materials Engineering, Iran University of Science and Technology, Tehran, Iran.
[2] Center for Electron Microscopy Research, Korea Basic Science Institute, Daejeon, Republic of Korea.
DOI: 10.22068/ijmse.15.3.1

Abstract: *the objective of this research was to investigate the microstructure of stabilized retained austenite from the Q&P heat treatment the primary goal of this heat treatment was to produce a microstructure consists of stabilized retained austenite and martensite. For this purpose, a low-alloy steel with 0.4wt. % carbon was treated by quench and partitioning (Q&P) process. The Q&P was conducted at different quenching temperatures to obtain a considerable amount of retained austenite, while partitioning temperature and time were kept constant. Using XRD profiles, volume percent, carbon concentration, and lattice parameters of retained austenite and martensite were calculated. At quenching temperature of 160°C, 12vol.% of austenite was stabilized at the room temperature, which was the highest amount achieved. The microstructural observations carried out on selected samples, revealed that retained austenite has a nanoscale particle size, about 200nm. Detection of retained austenite in the SEM micrographs became possible by utilizing SE2 signals via the difference in phases contrast. Two types of morphology, film-like and blocky type, were identified by means of TEM and TKD; a schematic model was proposed in order to explain these morphologies.*

Keywords: *Quench and Partitioning, Retained austenite, Nanoscale film-like RA, Low-alloy steel*

1. INTRODUCTION

Increasing attention has been paid in recent years to the development of steels containing considerable retained austenite (RA) in order to reach high strengths without substantial loss of toughness [1, 2]. Stabilizing austenite by carbon enrichment is known in the production of TRIP steels through rejection of carbon from bainite to austenite in the presence of alloying elements such as Si and Al which suppress the carbide precipitation during the austempering stage [3, 4]. With the purpose of improving mechanical properties in sheet steels, quench and partition (Q&P) heat treatment has developed, with the idea of creating a microstructure consisting of metastable retained austenite plus martensite [5, 6]. In this microstructure, metastable RA enhances strain hardening and when martensite is added tomicrostructure increase the strength of the alloy increases [7, 8].

Partitioning of carbon from supersaturated martensite into austenite is the principal for the carbon enrichment of austenite and consequently it's stabilization [9-11]. To succeed; Q&P process involves two essential steps. (1) Interrupted quench to a quench temperature (QT) between Ms and Mf to introduce a controlled amount of supersaturated martensite (initial martensite) as a carbon source to the microstructure. (2) Soaking at a designed partitioning temperature (PT) for a certain time (partitioning time, Pt) to enrich the untransformed austenite with carbon. At the end of the partitioning stage, steel would be quenched to the room temperature which results in the formation of fresh martensite in addition to stabilized retained austenite and diluted initial martensite. The fresh martensite transforms from the parts of the austenite that was not sufficiently enriched by carbon. It should be noted that a proper chemical composition must be chosen to suppress the competing reactions consuming carbon, like carbide precipitation and transformation of austenite to bainite or pearlite.

In previous studies, quench and partition heat treatment has been applied to different grades of steels, such as TRIP steels [12-14], martensitic stainless steels [7, 15-17] and CMnSi steels [18-

20]. Furthermore, some novel steels are specifically designed for the Q&P process [21-24]. It is interesting that the Q&P microstructure of martensitic stainless steels has coarser RA grains (>1.5μm) in comparison to the Q&P microstructure of other steels, which generally have nanoscale RA particles. Martensitic stainless steels are classified as high-alloy steels, while one of the main goals for designing steels for Q&P process is the production of low-alloy steels in order to reduce the production cost [1, 2, 25].

In the current research, a new low-alloy steel is designed, which, in contrast to the composition of steels used for Q&P heat treatment, Si was substituted with Ni, with the same purpose of suppressing cementite precipitation. The morphology, size, and distribution of nanoscale RA have been studied by means of various characterization techniques. A model has also been proposed to explain the observed morphologies of retained austenite after Q&P heat treatment.

2. EXPERIMENTAL PROCEDURE

A low alloy medium carbon steel with the composition shown in Table 1 was used in this research. Samples were cut from hot rolled sheets with 3 mm thickness. Dilatometry test performed to determine the critical temperatures Ac3 as well as M_s and M_f. The dilatometry tests were carried out on the specimens with dimensions of 10×5×1 mm3 in a Bahr805 pushrod dilatometer both in vacuum and in an Ar atmosphere.

For Q&P heat treatment, samples were fully austenitized in 850°C for 20 min and quenched in a salt bath furnace under different interrupted quench temperatures (QT) between M_s and M_f (i.e.140, 160, 180 and 200°C). Partitioning stage was carried out immediately by transferring the samples to another salt bath furnace at 300°C, in which they were kept for 1000 seconds. For simplicity, partitioning temperature and time, which were kept constant, were excluded from thev samples allocated names. Hence, samples are coded as QTx, in which x is the interrupted quench temperatures. The Q&P heat treatment route is shown in Fig. 1.

X-ray diffraction initially was used to determine the amount of retained austenite (RA) and then microstructural studies were conducted on selected samples with the highest amount of RA. X-ray patterns were recorded on Bruker D8 Advance X-ray diffractometer with Bragg-Brentano setup using Cu-Kα in the range of 40 to 100° (2θ) with a scanning rate of 0.5°/min and step size of 0.02° at 40 V. A graphite monochromator was used between sample and detector in order to avoid the fluorescence effect. Rietveld optimization method [26] was employed by MAUD software [20, 27] for analyzing X-ray patterns. The goodness of Fit (GOF) for these calculations was 1.5±0.4. The austenite lattice parameter (aγ) was calculated using Nelson-Riley extrapolation method [28] and carbon concentration in RA was estimated using the following equation [21, 29]:

$$a_\gamma=3.556+0.0453x_C+0.00095x_{Mn}-0.002x_{Ni} \quad (1)$$

in which, aγ is lattice parameter in Å, xC, xMn and xNi are respectively carbon, manganese and nickel content in weight percent.

Selected samples were used for obtaining images by scanning electron microscopy (SEM) technique. For more detailed examination, transmission Kikuchi diffraction (TKD), and transmission electron microscopy (TEM) analysis were conducted on the sample with the highest amount of RA. The microstructures were characterized by FE-SEM (Zeiss Ultra 55) after preparation by standard metallographic rout and using nital 4% + benzalkonium chloride (for better RA detection) as an etchant or by

Table 1. The chemical composition of designed steel (wt.%)

Fe	C	Ni	Mn	Si	Mo	Cr
Base	0.39	1.78	2.96	0.22	0.021	0.076

[DOI: 10.22068/ijmse.15.3.1]

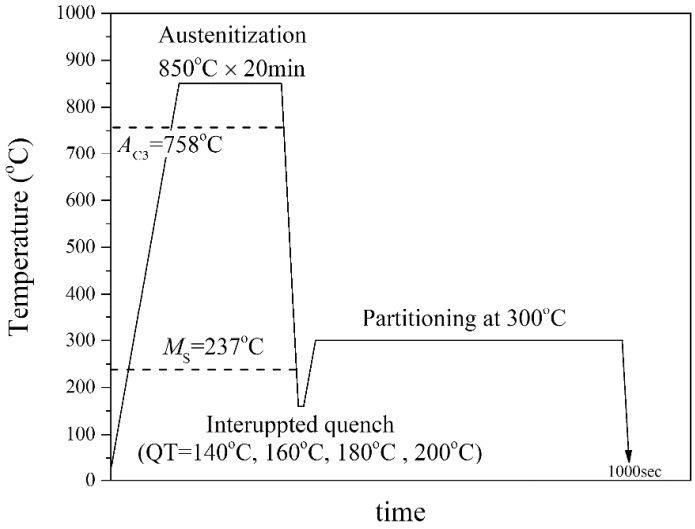

Fig. 1. Schematic representing two-step Q&P heat treatment route applied to specimens.

electropolishing with 8% $HClO_4$, 10% 2-ButoxyEthanol, 70% Ethanol, 12% distilled water at 40 V for 10 seconds. TKD and TEM samples were initially prepared by mechanical polishing down to 100 microns thickness, followed by twin-jet polishing using 10% $HClO_4$ as the electrolyte at the voltage of 30 V.

3. RESULTS AND DISCUSSION

3. 1. X-ray Analysis

X-ray patterns of 4 samples with different QTs but similar partitioning conditions are shown in Fig. 2. (200)γ, (220)γ and (311)γ peaks were observed in all patterns. The main peaks that are, (110)γ and (111)α, for γ-fcc and α-bcc respectively were overlapped. (111)α center peak position is detectable but in order to determine the (110)γ peak position, these two peaks were deconvoluted based on PearsonVII model; the deconvolution lines of the main austenite peak is shown in Fig. 2-b. QT200 peak was excluded from the results due to poor curve fitting.

The XRD patterns of the samples show an obvious shift in (200)α and (220)α towards higher 2θ values in QT160 and QT180 samples which can be attributed to smaller lattice parameter. This may be caused by the carbon partitioning from martensite to austenite which has led to a reduction of martensite lattice parameter. On the contrary, (111)γ peaks positions have shifted to lower values in Fig. 2-b. These peaks which are located at 44.441°, 43.817° and 43.915° for QT140, QT160 and QT180 samples, respectively show that QT160 has the highest lattice parameter whereas the QT140 has the lowest. The shift in austenite and martensite peaks confirm the carbon partitioning from martensite to austenite. However, it is interesting to saw that (110)α and (211)α peaks do not exhibit a similar trend which can be explained by two reasons: (1) The shift in peaks position may be related to martensite bct lattice since . Carbon has a much bigger influence on lattice parameter in z-direction in martensite. Therefore, the planes in z-direction such as (200)α cam be mostly affected by carbon partitioning. In these samples, maximum peak shift for (111)α was 0.11 while the shift for (200)α peak was 0.35. (2) This can also be attributed to co-existence of the initial and the newly formed martensite, since during partitioning, initial martensite can be formed in carbon rich area whereas the formation of fresh martensite if enough carbon supply would be available. This difference in the initial and the fresh martensite has been described in details in carbon constrained equilibrium (CCE) model [5, 12]. The model determines an optimum QT,

[DOI: 10.22068/ijmse.15.3.1]

above which carbon source for the enrichment of untransformed austenite is relatively low and below that temperature the fraction of initial martensite is high the amount of untransformed austenite be reduced. According to the calculated RA fraction from XRD results shown in Fig. 3, QT = 160°C was the optimum temperature for the studied steel. At this temperature, the maximum percentage of RA was 12%, and the amount of soluble carbon in austenite was estimated to be about 0.63 wt.%, on the base of equation 1.

Accordingly, for QT140 the amount of initial martensite which was tempered during partitioning was higher in comparison to other samples; and since it has undergone recovery, this phase will exhibit lower internal strain. For QT180 and QT200 samples, the amount of initial martensite which acted as the source of carbon was low. Therefore, carbon content in newly formed martensite was almost equal to the carbon content of the original It can be seen from Fig. 2-b that the main peak for QT180 is close to the

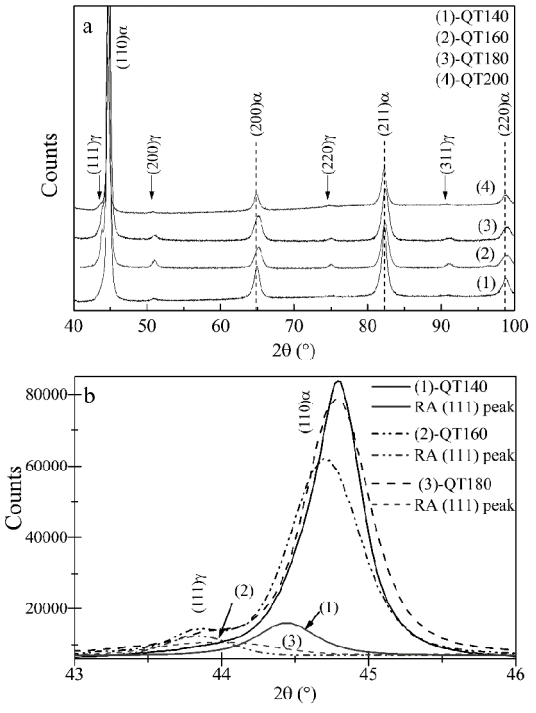

Fig. 2. (a) X-ray diffraction pattern of Q&P samples quenched to different QT. (b) Deconvolution lines of (111)γ and (110)α main peaks.

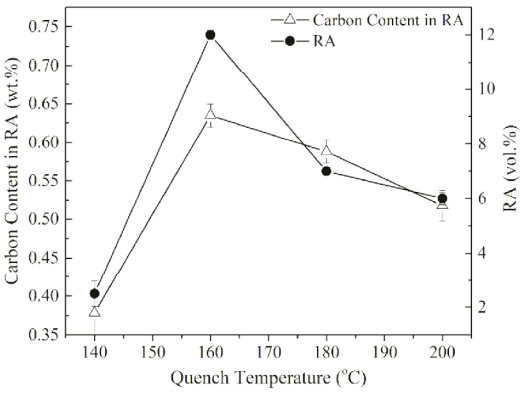

Fig. 3. Retained austenite carbon content and vol.% as a function of quench temperature.

QT140 peaks. For QT160, the amount of initial martensite as the source of carbon was sufficient which resulted in carbon-enriched fresh martensite. This has shifted both (110)α and (111)γ peaks for QT160 sample to the lower values compared to the other samples.

In an attempt to obtain a better understanding of the microstructure, XRD peak breadth for austenite and ferritic phases was studied with the results represented in Fig. 4. Chemical composition and grain size of RA can cause peak broadening. Distribution of carbon in austenite during partitioning is not uniform, i.e., during the partitioning, a chemical gradient will occur inside the austenite grains which leads to the peak broadening [28]. On the other hand, stabilized austenite divides the microstructure into smaller areas, therefore a finer fresh martensite will form. Hence, broadening can be also observed in ferritic phase peaks. This can explain the broader (110)α peak for QT160 compared to other samples.

The full width at half maximum (FWHM) has been used in this research as an indication of peak broadening. Fig. 4 shows the FWHM for (a) ferritic phases and (b) austenite. In order to eliminate the effect of instrumental broadening, calculations were done using the following equation: $FWHM^2 = FWHM^2_{obs} - FWHM^2_{inst}$. The α peaks of QT160 and QT180 showed the most peak broadening compared to other samples which were related to the presence of fresh

[DOI: 10.22068/ijmse.15.3.1]

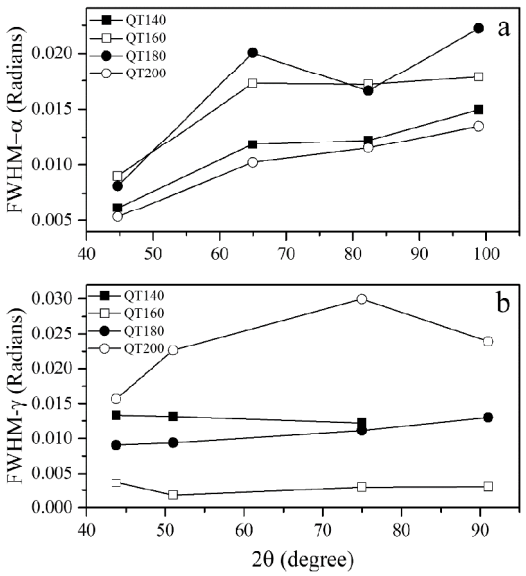

Fig. 4. FWHM values of (a) α and (b) γ peaks for Q&P samples.

martensite with smaller grain size and non-uniform internal strain (Fig. 4-a). As it is indicated in Fig. 4-b, RA peaks for QT160 and QT180 are sharper in comparison to QT140 and 200. Moreover, in these samples, FWHMγ did not change significantly with increasing the 2θ.

Williamson-Hall equation [30] was used to calculate the crystallite size and internal strain for RA and ferritic phases:

$$B\cos(\theta) = \frac{K\lambda}{D} + 2\varepsilon\sin(\theta) \qquad (2)$$

Where B is the peak broadening which is equivalent to FWHM in radians, D is crystallite size, ε is the non-uniform internal strain, K is Scherer's constant and λ is X-ray wavelength (Cu-Kα = 1.54059Å). Fig. 5 illustrates the crystallite size and non-uniform internal micro-strain for RA and α-phases in the Q&P samples.

For QT160 with the highest amount of RA (12%), crystallite size was around 200nm while for QT180 with 7% RA, crystallite size was about 75nm. Moreover, it can be seen in Fig. 5-a, that εγ in both samples was very small. The Dγ for QT200 with ~6% RA was estimated to be 40nm; besides, the peak broadening was the highest for this sample (Fig. 4-b), suggesting both small size and non-uniform strain in contrast to QT160 & QT180, were taking part in the peak broadening. In spite of the 2% calculated amount of RA for QT140 which is close to the instrumental limit of XRD detection, the non-uniform strain, εγ was negative which can be explained by the fact that in this specific sample the carbon content of RA was less than overall carbon content of the steel (Fig. 3). With the highest volume of RA and largest RA crystallite size, QT = 160°C can be considered as the optimum quenching temperature to stabilize austenite.

The size (Dα) and the non-uniform strain (εα) for α-phases depend on the amount of stabilized RA and carbon content. As explained before, a higher amount of stabilized austenite results to smaller fresh martensite at final quenching. Also, fresh martensite that forms from enriched austenite is richer in carbon, which increases the internal strain. This can explain the trend of the size and strain changes in α-phases shown in Fig. 5-b.

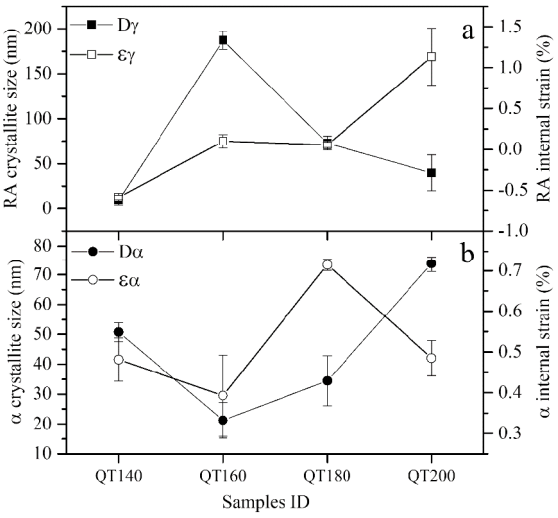

Fig. 5. The change in average crystallite size and internal strain with quench temperature for (a) austenite and (b) Ferritic phases.

[DOI: 10.22068/ijmse.15.3.1]

3. 2. Microstructural Studies

The main objective of Q&P heat treatment is to stabilize austenite in order to benefit from the ductility and work hardening properties of RA [7, 8]. Since QT160 and QT180 showed the highest amount of RA, 12% and 7% respectively, they were considered for the microstructural studies. Fig. 6 shows SEM micrographs for QT160 (a, b) and QT180 (c, d). The main feature in the images is the very fine microstructure constituents (RA and martensite) which are in agreement with the XRD analysis results. Instances of RA, martensite packets and bainitic ferrite (BF) are shown in Fig. 6. Comparing QT160 and QT180, it can be seen that bainitic ferrite grains are coarser in QT160. It has been shown that the presence of martensite can aid austenite to bainite transformation during partitioning [23]; hence a high amount of initial martensite, like what exist in QT160 in comparison with QT180, can be accounted for the coarser bainitic ferrite observed in the lower quench temperatures.

The micrographs were taken by SE2 detector which can collect both secondary (SE) and backscattered (BSE) electrons. In this way, phase contrasts resulted from BSE can help in distinguishing austenite from ferritic phases. In Fig. 6, the fine constituents with bright contrast which are distributed between martensite laths are retained austenite. By exploiting the contrast difference between austenite and ferritic phases, quantitative analysis using image analyzer software has became possible. Due to the fine microstructure constituents, analysis has been carried on the 10k and 25k magnification micrographs which were used to determine the RA amount and average size, respectively. RA volume percent of 13.6 ± 2.2 and RA size of 180 ± 30nm are calculated for QT160 and RA volume percent of 9.0 ± 1.6 and RA size of 114 ± 25 nm were calculated for QT180. This difference in RA size seems to be due to the different amount of initial martensite as a carbon source in QT160

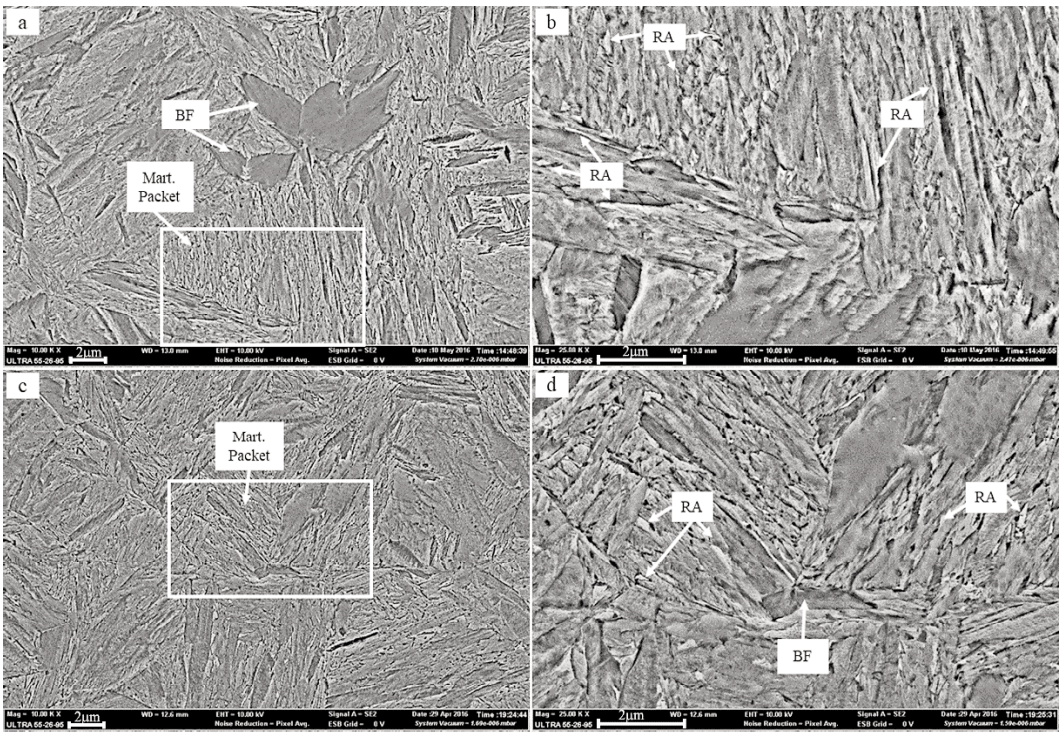

Fig. 6. SEM micrographs of (a) and (b) QT160, (c) and (d) QT180. Images b and d are displaying higher magnification of boxed areas. Some instances of retained austenite (RA) and bainitic ferrite (BF) are shown.

[DOI: 10.22068/ijmse.15.3.1]

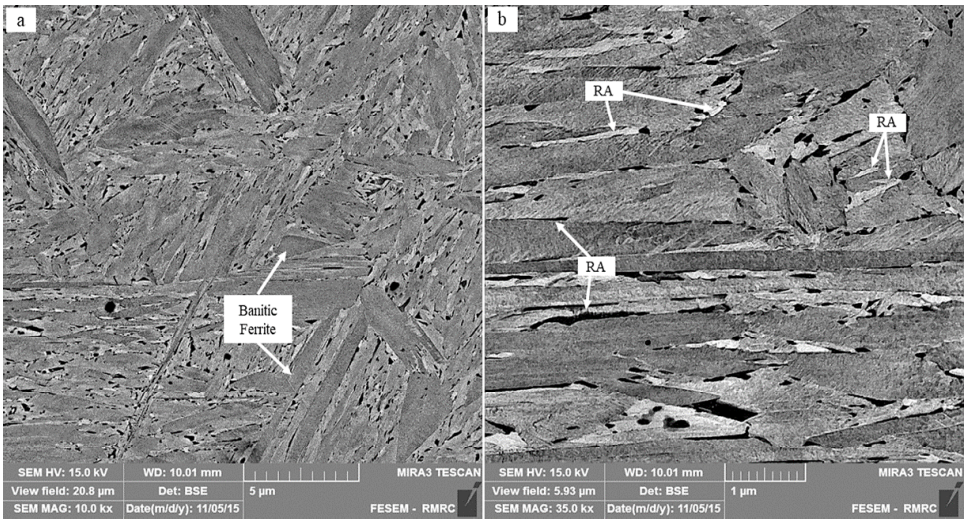

Fig. 7. The microstructure of electropolished sample (QT160) obtained by BSE-SEM. In the micrographs, along with the bright fine phases, removed areas are also retained austenite which were removed during electropolishing.

and QT180 samples, which influences RA stabilization. RA volume resulted from analyzing micrographs are in good agreement with XRD results.

In addition to the etching techniques, electropolishing can be used to reveal the microstructure by utilizing backscattered electrons in SEM and EBSD [17, 31, 32]. Fig. 7 shows the BSE-SEM microstructure of QT160 prepared by electropolishing without any further etching. Although the electropolishing time was relatively short (10 sec), the reveal of austenite is still evident, as shown shown in Fig. 7-b. Worth mentioning, this figure shows that the most of retained austonite has been desolved from the surface of microstructure during electropolishing, i.e. black areas. including bright contrast and removed areas. According to the size and shape of the removed areas, it can be concluded that austenite is more sensitive to electropolishing effect compared to strained ferritic phases (i.e.martensite and bainitic ferrite). Regardless of RA removal during electropolishing, the size and distribution of RA particles can still be recognized in the microstructure.

In order to further investigate the morphology of RA, TKD and TEM were used. TKD method which is also known as t-EBSD can be used for analysis of nanoscale grains [33-35]. Pattern

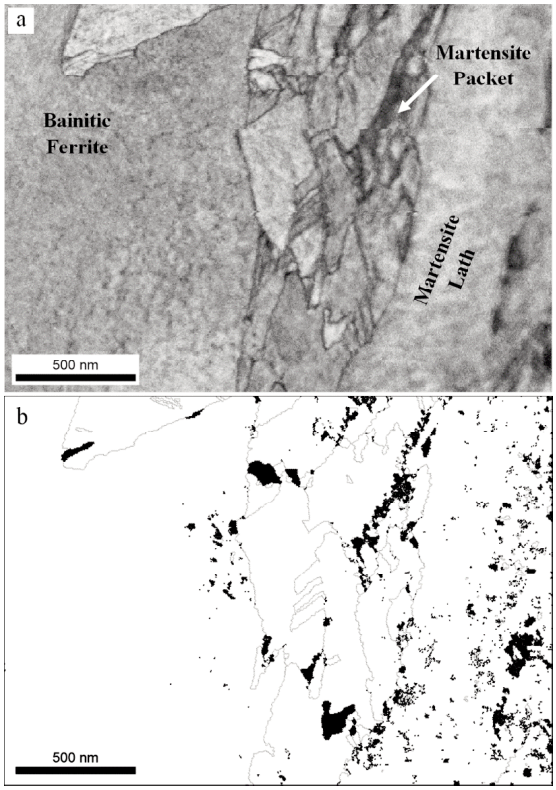

Fig. 8. Transmission Kikuchi diffraction images from QT160 showing (a) pattern quality image and (b) austenite phase map with high angle grain boundaries.

[DOI: 10.22068/ijmse.15.3.1]

quality (PQ) image (a) and austenite phase map (b) obtained by TKD at 50k magnification are shown in Fig. 8. A bainite grain and a martensite packet are shown in the PQ image and blocky and film-like retained austenite grains are shown in the Euler map.

Fig. 9 shows the TEM micrographs of QT160 with three parent austenite grains which their boundaries meet at triple-point (T-P). A martensite packet and bainitic ferrite grains are also shown. Considering these phases as a reference in the dark field (DF) images (b and c), the position of RA particles can be well detected. Retained austenite particles can be seen in the Fig. 9-c which is taken with (020)γ diffraction point in the selected area electron diffraction (SAED) pattern shown in Fig. 9-d. This image confirms that RA has a nanoscale particle size and are located between martensite laths and bainite grain boundaries. Zone axis in the SAED pattern is equal to [101]γ and [111]α directions; also, it can be seen that {111}γ and {011}α planes are parallel. The SAED pattern reveals that Kurdjumov-Sachs relationship exists between the martensite and RA. The K-S relation is reasonable since the steel is low alloyed and has 0.39wt.% carbon. Moreover, the maximum amount of carbon in the fresh martensite would be equal to the carbon enriched retained austenite which is about 0.63 wt.%. This amount of carbon in the martensite is in the range, in which the K-S relation is more probable than the other relationships [36].

TKD and TEM studies confirmed the morphology and size of RA which were discovered in SEM images. Both film-like and blocky type morphologies of retained austenite were identified in the microstructure resulted

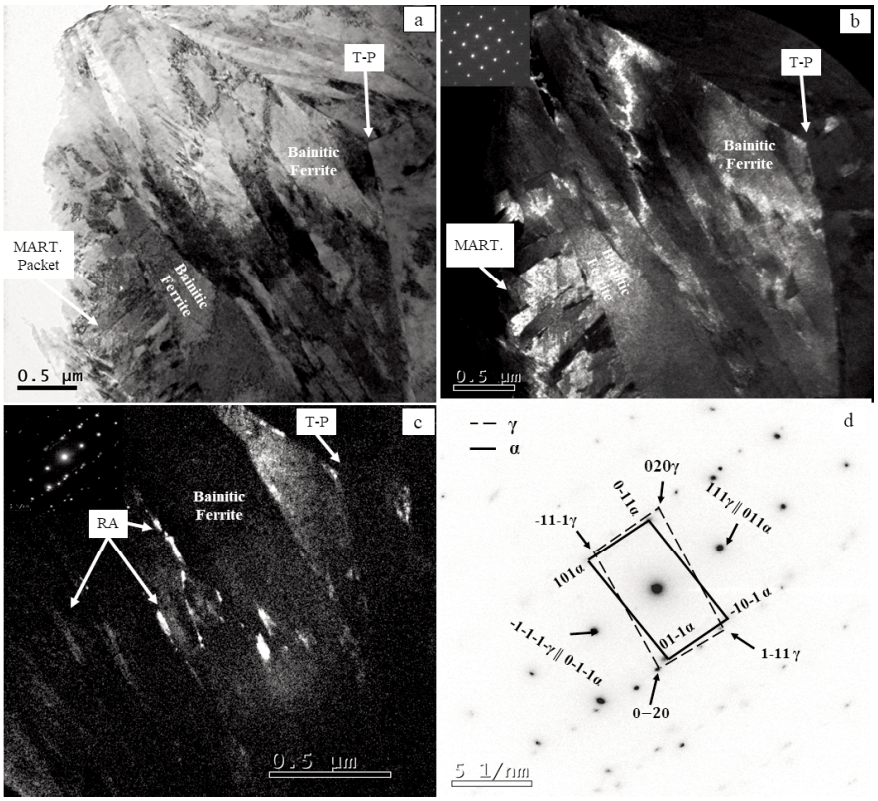

Fig. 9 TEM micrographs of QT160 displaying prior austenite grain boundaries meet at a triple point (T-P). (a) BF image, (b) DF image taken with $(01\bar{1})\alpha$ reflection, (c) DF image of RA taken with $(0\bar{2}0)\gamma$ reflection and (c) corresponding SAED pattern showing K-S relationship between martensite and RA.

[DOI: 10.22068/ijmse.15.3.1]

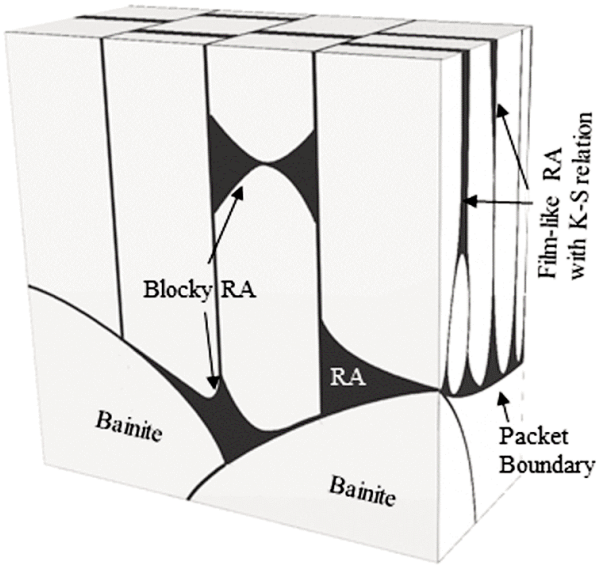

Fig. 10. Schematic model illustrating the blocky and film-like morphologies of retained austenite between martensite laths and bainite grain boundaries.

from Q&P heat treatment. The film-like morphology of the RA located between martensite laths because, at the initial times of partitioning step, carbon is rejected to the martensite-austenite interface and then starts to partition into the untransformed austenite. Therefore, by moving further from the interface, a carbon concentration gradient was generated; consequently, only a small area near the interface can be sufficiently enriched with carbon in order to stabilize austenite, thus a film-like morphology was formed. On the other hand, blocky type RAs needs further explanation.

In order to explain the nanoscale blocky RA particles, a schematic model has been proposed which is presented in Fig. 10. Based on this model, these blocky type RAs can be either the cross section of film-like RA particles or the grains which remain due to constraints in martensitic and bainitic transformations. Considering the TKD image in Fig. 8-b, one may say that the blocky type RA particles are located inside a martensite packet with the side view cross-section. This martensite packet is similar to the structure illustrated in the front view plane in the schematic model. In view of all microstructural studies, it can be concluded that in the Q&P microstructure, retained austenite mainly has the film-like morphology.

4. CONCLUSIONS

Quench and partitioning heat treatment has been successfully applied to a newly designed low-alloy medium-carbon steel. The quenching temperature (QT) was the only variable and partitioning parameters (PT =300°C & Pt=1000 sec) were kept constant. Retained austenite (RA) size, morphology, and distribution were studied. The results can be summarized as follow:

1. The steel composition designed for Q&P heat treatment was successfully prevented from cementite formation in the selected partitioning conditions. The final microstructure consists of martensite, retained austenite and bainitic ferrite.
2. By means of SE2 and BSE signals in SEM imaging, it became possible to recognize nanoscale retained austenite and eventually quantifying the RA via image analysis. Combining with the peak broadening analysis of XRD patterns, it has been shown that retained austenite grains have

[DOI: 10.22068/ijmse.15.3.1]

nanoscale size up to 200nm

3. XRD analysis showed that the crystallite size of retained austenite was about 200nm for the sample with the highest amount of RA, which was close to the RA grain size calculated by image processing technique. The highest RA volume percentage obtained at quench temperature of 160°C was 12 vol.%.
4. TKD and TEM analysis were showed two types of morphology, film-like and blocky type of retained austenite, with the film-like being the main morphology. Also, it is found that martensite was formed with the K-S relationship to retained austenite.
5. A physical model proposed to explain the retained austenite observed morphologies.

REFERENCES

1. Matlock, D. K. and Speer, J. G., "Third Generation of AHSS: Microstructure Design Concepts", in Microstructure and Texture in Steels and Other Materials, Springer, 2009, 185-205.
2. Weng, Y., Dong, H. and Gan, Y., Eds, "Advanced Steels: The Recent Scenario in Steel Science and Technology.", Springer, 2011.
3. Li, L., Wollants, P., He, Y. L., DeCooman, B. C., Wei, X. C. and Xu, Z. Y., "Review and Prospect of High Strength Low Alloy TRIP Steel, Acta Metall". Sin. (English Letters), 2003, 16, 457-465.
4. Zrnik, J., Mamuzić, I. and Dobatkin, S. V., "Recent progress in high strength low carbon steels.", Metalurgija, 2006, 45, 323-331.
5. Speer, J. G., Assunção, F. C. R., Matlock, D. K. and Edmonds, D. V., "The quenching and partitioning process: background and recent progress", Mat. Res., 2005, 8, 417-423.
6. Edmonds, D.V., He, K., Rizzo, F.C., De Cooman, B.C., Matlock, D.K. and Speer, J.G., Quenching and partitioning martensite—A novel steel heat treatment, Mater. Sci. Eng. A,2006, 438–440, 25-34.
7. De Moor, E., Lacroix, S., Clarke, A. J., Penning, J. and Speer, J. G., "Effect of retained austenite stabilized via quench and partitioning on the strain hardening of martensitic steels"., Metall. Mater. Trans. A, 2008, 39, 2586-2595.
8. Speer, J. G., De Moor, E., Findley, K. O., Matlock, D. K., De Cooman, B. C. and Edmonds, D. V., "Analysis of Microstructure Evolution in Quenching and Partitioning Automotive Sheet Steel", Metall. Mater. Trans. A, 2011, 42, 3591-3601.
9. Speer, J., Matlock, D. K., De Cooman, B. C. and Schroth, J. G., "Carbon partitioning into austenite after martensite transformation", Acta Materialia, 2003, 51, 2611-2622.
10. Speer, J. G., Edmonds, D. V., Rizzo, F. C. and Matlock, D. K., "Partitioning of carbon from supersaturated plates of ferrite, with application to steel processing and fundamentals of the bainite transformation", Curr. Opin. Solid State Mater. Sci., 2004, 8, 219-237.
11. Clarke, A. J., Speer, J. G., Matlock, D. K., Rizzo, F. C., Edmonds, D. V. and Santofimia, M. J., "Influence of carbon partitioning kinetics on final austenite fraction during quenching and partitioning", Scripta Mater., 2009, 61, 149-152.
12. Clarke, A. J., Speer, J. G., Miller, M. K., Hackenberg, R. E., Edmonds, D. V., Matlock, D. K., Rizzo, F. C., Clarke, K. D. and De Moor, E., "Carbon partitioning to austenite from martensite or bainite during the quench and partition (Q&P) process: A critical assessment", Acta Mater., 2008, 56, 16-22.
13. Santofimia, M. J., Zhao, L., Petrov, R. and Sietsma, J., "Characterization of the microstructure obtained by the quenching and partitioning process in a low-carbon steel", Mater. Charact., 2008, 59, 1758-1764.
14. Santofimia, M. J., Speer, J. G., Clarke, A. J., Zhao, L. and Sietsma, J., "Influence of interface mobility on the evolution of austenite–martensite grain assemblies during annealing", Acta Mater., 2009, 57, 4548-4557.
15. Tobata, J., Ngo-Huynh, K. L., Nakada, N., Tsuchiyama, T. and Takaki, S., "Role of Silicon in Quenching and Partitioning Treatment of Low-carbon Martensitic Stainless Steel", ISIJ Int., 2012, 52, 1377–1382.
16. Tsuchiyama, T., Tobata, J., Tao, T., Nakada, N. and Takaki, S., "Quenching and partitioning treatment of a low-carbon martensitic stainless steel", Mater. Sci. Eng., A, 2012, 532, 585-592.

[DOI: 10.22068/ijmse.15.3.1]

17. Mola, J. and De Cooman, B. C., "Quenching and Partitioning (Q&P) Processing of Martensitic Stainless Steels", Metall. Mater. Trans. A, 2013, 44, 946-967.
18. De Moor, E., Speer, J. G., Matlock, D. K., Kwak, J. H. and Lee, S. B., "Effect of Carbon and Manganese on the Quenching and Partitioning Response of CMnSi Steels", ISIJ Int., 2011, 51, 137-144.
19. Hauserová, D., Duchek, M., Dlouhý, J. and Nový, Z., "Properties of Advanced Experimental CMnSiMo Steel Achieved by QP Process", Procedia Eng., 2011, 2961-2966.
20. Gao, G., Zhang, H., Gui, X., Tan, Z. and Bai, B., "Tempering Behavior of Ductile 1700 MPa Mn–Si–Cr–C Steel Treated by Quenching and Partitioning Process Incorporating Bainite Formation", J. Mater. Sci. Technol. (Shenyang, China), 2015, 31, 199-204.
21. Santofimia, M. J., Zhao, L., Petrov, R., Kwakernaak, C., Sloof, W. G. and Sietsma, J., "Microstructural development during the quenching and partitioning process in a newly designed low-carbon steel", Acta Mater., 2011, 59, 6059-6068.
22. Liu, S. G., Dong, S. S., Yang, F., Li, L., Hu, B., Xiao, F. H., Chen, Q. and Liu, H. S., "Application of quenching–partitioning–tempering process and modification to a newly designed ultrahigh carbon steel", Mater. Des., 2014, 56, 37-43.
23. Guo, H., Gao, G., Gui, X., Misra, R. D. K. and Bai, B., "Structure-property relation in a quenched-partitioned low alloy steel involving bainite transformation", Mater. Sci. Eng., A, 2016, 667, 224-231.
24. Wang, C. Y., Chang, Y., Jie, Y. A. N. G., Cao, W. Q., Han, D. O. N. G. and Wang, Y. D., "Work Hardening Behavior and Stability of Retained Austenite for Quenched and Partitioned Steels", J. Iron Steel Res. Int, 2016, 23, 130-137.
25. Grajcar, A., Kuziak, R. and Zalecki, W., "Third generation of AHSS with increased fraction of retained austenite for the automotive industry", Arch. Civ. Mech. Eng, 2012, 12, 334-341.
26. McCusker, L. B., Von Dreele, R. B., Cox, D. E., Louër, D. and Scardi, P., "Rietveld refinement guidelines", J. Appl. Crystallogr., 1999, 32, 36-50.
27. Lutterotti, L., Wenk, H. and Matthies, S., "MAUD (material analysis using diffraction): a user friendly Java program for Rietveld texture analysis and more", Proceeding of the twelfth international conference on textures of materials (ICOTOM-12), Ottowa, Canada, 1999, 1599-1604.
28. Waseda, Y., Matsubara, E. and Shinoda, K., "X-ray diffraction crystallography: introduction, examples and solved problems". Springer Science & Business Media, 2011, 120-121
29. Cullity, B. D. and Stock, S. R., "Elements of X-ray Diffraction"., NJ, USA, 2001, 352.
30. Brandstetter, S., Derlet, P. M., Van Petegem, S. and Van Swygenhoven, H., "Williamson–Hall anisotropy in nanocrystalline metals: X-ray diffraction experiments and atomistic simulations", Acta Mater., 2008, 56, 165-176.
31. Zaefferer, S., Romano, P. and Friedel, F., "EBSD as a tool to identify and quantify bainite and ferrite in low alloyed Al TRIP steels", J. Microsc. (Oxford), 2008, 230, 499-508.
32. Chen, Y., Hjelen, J., Gireesh, S. S. and Roven, H. J., "Optimization of EBSD parameters for ultra-fast characterization", J. Microsc. (Oxford), 2012, 245, 111-118.
33. Trimby, P. W., Cao, Y., Chen, Z., Han, S., Hemker, K. J., Lian, J., Liao, X., Rottmann, P., Samudrala, S., Sun, J. and Wang, J. T., "Characterizing deformed ultrafine-grained and nanocrystalline materials using transmission Kikuchi diffraction in a scanning electron microscope", Acta Mater., 2014, 62, 69-80.
34. Abbasi, M., Kim, D. I., Guim, H. U., Hosseini, M., Danesh-Manesh, H. and Abbasi, M., "Application of Transmitted Kikuchi Diffraction in Studying Nano-oxide and Ultrafine Metallic Grains, ACS Nano, 2015, 9, 10991-11002.
35. Mortazavi, N., Esmaily, M. and Halvarsson, M., "The capability of Transmission Kikuchi Diffraction technique for characterizing nano-grained oxide scales formed on a FeCrAl stainless steel", Mater. Lett., 2015, 147, 42-45.
36. Bhadeshia, H. K. D. H. and Honeycombe, R. W. K., "Steels Microstructure and Properties", Third Edition ed., Oxford, UK, 2006, 110-112.

[DOI: 10.22068/ijmse.15.3.1]